Applied Geochemistry 84 (2017) 277–285

Contents lists available at ScienceDirect

Applied Geochemistry

journal homepage: www.elsevier.com/locate/apgeochem

Trace element and U isotope analysis of uraninite and ore concentrate: Applications for nuclear forensic investigations

Tyler L. Spano [a, *], Antonio Simonetti [a], Enrica Balboni [a, b], Corinne Dorais [a], Peter C. Burns [a, c]

[a] Department of Civil and Environmental Engineering and Earth Sciences, University of Notre Dame, Notre Dame, IN, 46556, United States
[b] Glenn T. Seaborg Institute, Physical and Life Science Directorate, Lawrence Livermore National Laboratory, 7000 East Avenue, Livermore, CA, 94550, United States
[c] Department of Chemistry and Biochemistry, University of Notre Dame, Notre Dame, IN, 46556, United States

ARTICLE INFO

Article history:
Received 9 February 2017
Received in revised form
22 June 2017
Accepted 3 July 2017
Available online 11 July 2017

Editorial Handling by Prof. M. Kersten.

Keywords:
Uranium ore concentrate
Uraninite
ICP-MS
REE
Nuclear forensics

ABSTRACT

Uranium ore concentrate (UOC), is an important intermediate material in the nuclear fuel cycle. Trace element distributions in UOCs can be related to the geologic conditions in which the source uranium ore formed, and hence are characteristic for each deposit type. These chemical signatures can then potentially be used as an essential tool for nuclear forensic analysis of derivative radioactive materials. In this study, several samples of UOC and uraninite extracted from sandstone-hosted roll front deposits in the Powder River basin U province in Wyoming (USA) have been analyzed for their trace element abundances and U isotopic compositions. UOCs were analyzed both in solution mode-inductively coupled plasma mass spectrometry (SM-ICP-MS) subsequent bulk sample digestion, and at high-spatial resolution (10s of micron scale) using a laser ablation (LA)-ICP-MS technique. Comparison of trace elemental abundances obtained by SM- and LA-ICP-MS indicates corroborating results, with comparable chondrite-normalized rare earth element (REE) patterns; those obtained by LA-ICP-MS show a slightly larger variation in absolute elemental abundances compared with corresponding bulk sample digestions. U isotopic measurements for UOCs and uraninite were conducted by solution mode multi-collector (MC)-ICP-MS. $^{238}U/^{235}U$, $^{235}U/^{234}U$ and $^{238}U/^{234}U$ ratios for uraninite and UOC overlap and confirm a lack of significant isotopic fractionation during the fabrication process. The results reported here assert the validity of analyzing UOC for source attribution purposes and simultaneously demonstrate that corroborating trace element signatures can be obtained with both LA and SM-ICP-MS analytical techniques for U-rich materials relevant to the nuclear fuel cycle. REE abundances and U isotopes did not fractionate during early ore processing of materials investigated in this study.

1. Introduction

1.1. Nuclear forensics

Between 1993 and 2001, more than 2150 incidents of illicit trafficking of radioactive materials were recorded by the International Atomic Energy Agency (IAEA, 2006). Of these incidents, > 400 involved physical nuclear material such as depleted, natural, or low-enriched uranium. The goal of nuclear forensic analysis is to attribute, using forensic indicators, interdicted materials to a source or sources thereby thwarting actions that would utilize illicit nuclear material and to monitor compliance with the Nuclear Nonproliferation Treaty (United Nations, 1968). Nuclear forensics exploits the fact that certain measureable parameters or signatures are unique with respect to the geologic origin of a sample of interest. Types of critical evidences sought for forensic purposes include isotopic information, age data, and trace element compositions (IAEA, 2006, 2014; American Physical Society, 2008).

Rare earth elements (REEs) readily incorporate in uraninite (UO_2), the principal natural U ore source for derivative nuclear material such as uranium ore concentrate (UOC). This is attributed to similarities between the ionic radii of U^{4+} in eight-fold coordination and the preferred coordination environment of REEs (Finch and Murakami, 1999). In addition to elemental availability in parent

* Corresponding author.
E-mail address: tspanofr@nd.edu (T.L. Spano).

http://dx.doi.org/10.1016/j.apgeochem.2017.07.003
0883-2927/

magmas and fluids, variations in REE concentrations within uraninite may be governed by ore genesis and alteration temperatures, but also influenced by mineral cogenesis and preferential leaching of REEs during alteration events (Frimmel et al., 2014; Fryer and Taylor, 1987; Mercadier et al., 2011). Consequently, source attribution through analysis of REE in radioactive materials has been the focus of numerous studies in the realm of nuclear forensics (Boulyga et al., 2015; Depiné et al., 2013; Dhana Raju and Babu, 2003; Fleischer and Altschuler, 1969; Frimmel et al., 2014; Fryer and Taylor, 1987; Han et al., 2013; Horie et al., 2010; Keegan et al., 2012; Lach et al., 2013; Mercadier et al., 2011; Premadas and Srivastava, 2002; René, 2008; Švedkauskaite-legore et al., 2007; Varga et al., 2010; Walters et al., 2013). REE analysis has been described as the most efficient tool for defining the geologic provenance of uraninite (Depiné et al., 2013; Fryer and Taylor, 1987; Mercadier et al., 2011). Moreover, U, Sr, and Pb isotopic signatures have been used to delineate the origin and age of U-rich materials (Balboni et al., 2016; Mayer et al., 2007; Mayer et al., 2005).

1.2. Nuclear forensics methodology

1.2.1. Trace element signatures in uraninite

Analysis of nuclear materials for REE content commonly utilizes chondrite normalized (CN) plots as a means to identify geologic processes involved with the formation of primary ore materials. Normalizing REE abundances of samples negates the Oddo-Harkins effect associated with varying primordial-Earth REE concentrations (McDonough and Sun, 1995). Hence, the patterns of the resulting CN-REE curves are characteristic of the geologic processes responsible for their formation and can be used to identify the source and genetic type of U ore and associated minerals (Balboni et al., 2016; Bowie, 1979; Dahlkamp, 1993; Fleischer and Altschuler, 1969; Frimmel et al., 2014; Fryer and Taylor, 1987; Keegan et al., 2014, 2008, 2012; Krajkó et al., 2016; Lach et al., 2013; Mercadier et al., 2011; Premadas and Srivastava, 2002; Švedkauskaite-legore et al., 2007; Varga et al., 2010).

1.2.2. Previous studies: trace element analysis as a forensic indicator

CN-REE signatures of uraninite from numerous provinces of varied geologic origin worldwide have been investigated (Frimmel et al., 2014; Mercadier et al., 2011), and are used to observe distinct differences in the shapes of these signatures. REE partitioning plots are utilized to relate the fractions of light (La-Gd) and heavy (Tb-Lu) REEs (Frimmel et al., 2014). This type of investigation is useful for determining initial and/or alterations temperatures as incorporation of REEs within uraninite is heavily influenced by temperature (Frimmel et al., 2014; Mercadier et al., 2011).

REE analysis of UOCs has shown that trace element signatures from the parent uranium ore persist at this stage of the fuel cycle despite being precipitated from leach solutions (Keegan et al., 2014, 2008, 2012; Varga et al., 2010). For example, Australian UOCs derived from the Beverley, Ranger, and Olympic Dam deposits were correctly identified as originating from sandstone, unconformity-related, and breccia complex deposit types, respectively (Keegan et al., 2008). Similar analyses are needed to investigate REE signatures in North American U ores and corresponding ore concentrates originating from sandstone-hosted deposits. Sandstone-hosted U is of significant economic importance in the United States, and accounts for approximately 41% of known U deposits worldwide (IAEA, 2014).

Dustin et al. (2016) recently explored the merit of method validation by analyzing identical nuclear samples using differing sample introduction techniques typically employed with inductively coupled plasma mass spectrometry (ICP-MS). Aliquots of Trinitite, post-detonation debris from the first atomic bomb test, were analyzed using both laser ablation (LA) and solution mode (SM-ICP-MS) with corroborating results (Dustin et al., 2016). Digestion of bulk samples followed by preparation for SM-ICP-MS analysis is both time-consuming and labor intensive. In contrast, LA-ICP-MS analysis is advantageous due to the ability of obtaining spatially resolved data and requires far less sample preparation (a vast majority of samples can be ready for analysis within 24 h). The appealing prospect of decreasing sample preparation times for nuclear forensic analysis from the order of days or weeks (solution mode) to <1 day (laser ablation) benefits from further method validation and proof of concept, which are attainable via parallel analyses of other forms of nuclear material. For this reason, we conducted a comparative study of the elemental abundances obtained by SM-ICP-MS analyses on bulk samples of uraninite and UOCs, versus those obtained in-situ by LA-ICP-MS for the identical materials.

1.2.3. U isotope analysis for nuclear forensics

Recent advances in multicollector (MC)-ICP-MS instrumentation, such as the development and use of a multiple array of secondary electron multipliers, have aided in the simultaneous acquisition of multiple ion signals in low level (nanogram to subnanogram) U-bearing samples, with high accuracy and precision (comparable to that obtained by thermal ionization mass spectrometry- TIMS) (Boulyga et al., 2016; Pollington et al., 2016). In turn, U isotope ratios in nuclear materials have been used to better understand the extent of redox sensitivity and post deposition alteration on UOC and uraninite (Brennecka et al., 2010; Stirling et al., 2007).

Mass dependent isotopic fractionation can result in observed permil-to percent level variations in $^{238}U/^{234}U$ (Bopp et al., 2010; Brennecka et al., 2010). Natural variability of this isotope system has been detected in low-temperature environments as a result of α-recoil damage of the uraninite crystal lattice, and subsequent preferential removal of ^{234}U by aqueous oxidative processes (Stirling et al., 2007). Variations in the $^{235}U/^{234}U$ ratio of natural samples have long been recorded particularly in seawater, and have also been attributed to α-recoil-induced crystalline instability and corresponding preferential removal of the lighter isotope (Brennecka et al., 2010). Depletions in ^{234}U relative to the heavier U isotopes can be indicative of preferential leaching and aqueous alteration of U ores, and may provide insight into whether deposition of U is ongoing or concluded (Brennecka et al., 2010). These isotope systems can thus provide evidence of temporal variations in U deposition and can elucidate the provenance and history of nuclear materials (Bigeleisen, 1996; Brennecka et al., 2010).

Isotopic partitioning in the $^{238}U/^{235}U$ system has also been observed in uraninite and is attributed to the preferential reduction of ^{238}U. This is the result of different availabilities of individual U nuclei to attract electrons caused by dissimilarities in neutron numbers for ^{238}U and ^{235}U. This so called nuclear field shift (NFS) results in increased concentrations of the heavy isotope in the reduced phase and is distinct from mass dependent isotopic fractionation (Abe et al., 2008; Bigeleisen, 1996; Brennecka et al., 2010). Faster reaction kinetics for ^{238}U has also been observed to lead to fractionation in the $^{238}U/^{235}U$ system and can also be attributed to NFS (Bopp et al., 2010). Dissimilarities in the mechanisms (mass dependent vs. NFS) which lead to U isotopic separation provide distinct and significant forensic evidence regarding the fluid interactions and redox-susceptibility of U ores and derivative materials (Bopp et al., 2010; Brennecka et al., 2010; Richter et al., 1999; Stirling et al., 2007).

2. Materials and methods

2.1. Samples

Two specimens of uraninite and four samples of UOC from the Willow Creek Project located within the Powder River Basin uranium province were investigated in this study (Fig. 1, Table 1). All samples originate from a sandstone-hosted roll-front type deposit (Dahlkamp, 1993). The latter are characterized by precipitation of disseminated uraninite and coffinite ($USiO_4$) at a reducing front, which is subsequently altered and involves precipitation of uranyl vanadate minerals. The reducing front in this deposit consists of detrital carbonaceous debris (Dahl and Hagmaier, 1976; Santos and Ludwig, 1983). The historical flow of U-rich fluids followed the topographical hydrologic gradient of this region and occurred in arkosic fluvial sandstones deposited within a sedimentary basin bounded by Precambrian granites (Finch, 1996). These granites and Oligocene volcanic ash are possible hypogene U sources (Davis, 1969).

U is extracted from the deposits via injection wells and separated from leaching solutions using anion exchange resins. Uranium is precipitated as uranyl peroxide from the eluent via several pH modifications followed by addition of hydrogen peroxide (Martin, 1980). Uranyl peroxide is washed, dewatered, dried and stored in steel drums. Samples of UOC were received as fine powders dark brown in color (Fig. 1a).

2.1.1. Sample preparation- trace element analysis

For SM-ICP-MS analysis, sample digestion and preparation took place in a class 1000 clean room facility. Three aliquots of approximately 50 mg of each of the four UOC samples were weighed and placed in pre-cleaned Savillex® Teflon beakers. For each sample, ~1 mL of double-distilled concentrated (16N) HNO_3 was added to the vessel. Samples were capped and heated at 110 °C for 48 h. Following initial digestion, samples were removed from the hotplate and cooled for one hour. The beaker was uncapped and any sample residue adhered to the sides of the beakers was rinsed with 18 MΩ water. Samples were heated at 150 °C to dryness (~24 h). Approximately 0.5 mL of double-distilled 16N HNO_3 was added to dried samples. The vessels were recapped and placed on the hotplate for 24 h at 110 °C. The beaker was again uncapped and rinsed with 18 MΩ water. Samples were heated at 150 °C to dryness over 24 h. This last step was repeated one more time. Once dry, ~0.5 mL of 16N HNO_3 was added to each beaker, and samples were immediately heated to dryness at 150 °C. Approximately 2.5 mL of 16N HNO_3 was added to dry samples and complete dissolution was noted by visual inspection. Dissolved samples were transferred to 125 mL polypropylene bottles and weighed. Ultrapure water was added to bottles until a total weight of approximately 100 g was reached. Samples were then analyzed for trace element concentrations using a spike addition method (after Jenner et al., 1990).

UOC samples were prepared for LA-ICP-MS analysis by loading four drops of epoxy with UOC powder. Epoxy-mounted samples were cured and polished with Al_2O_3 powder (1 μm) to expose sample powder. Polished samples were carbon-coated for electron microprobe analysis using a Cameca SX-50 (Fig. 1b and c). An acceleration voltage of 15 kV and 100 nA current was used with a 15 μm beam size. Standardizations were performed using well characterized in-house standards of uranium dioxide (UO_2), vanadium oxide (V_2O_3), and anorthite glass (CaO) (Balboni et al., 2016).

2.1.2. Sample preparation- U isotope measurements

Sample preparation for U isotopic investigations also took place in a class 1000 clean room facility and involved transferring dissolved aliquots of the UOC powders to pre-cleaned Savillex® Teflon beakers, which were subsequently placed on a hot plate at 110 °C and evaporated to dryness. Prior to U ion exchange chemistry, samples were re-dissolved into 2 mL double-distilled concentrated (16N) HNO_3 at 110 °C after which 10 mL of 3M HNO_3 was added. Evergreen Scientific 5" columns were rinsed with 18 MΩ water and loaded with 2 mL UTEVA (100–150 μm) resin. Columns were then primed with 10 mL 1M HCl and washed with 10 mL of 18 MΩ water. 15 mL of 3M HNO_3 was added to condition the columns prior to addition of 5 mL aliquots of sample. Following sample addition, columns were rinsed with 10 mL 3M HNO_3 followed by 9M HCl. Th is eluted to waste upon addition of 10 mL of 5M HCl and 0.05M $H_2C_2O_4$. U is then eluted to pre-cleaned Savillex® Teflon beakers upon addition of 15 mL 1M HCl. U samples are then evaporated to dryness at 110 °C and then re-dissolved into 1 mL double-distilled concentrated (16N) HNO_3 at 110 °C (Pollington et al., 2016). Samples are then diluted in 2% HNO_3 to ~50 ppb solutions for MC-ICP-MS analysis.

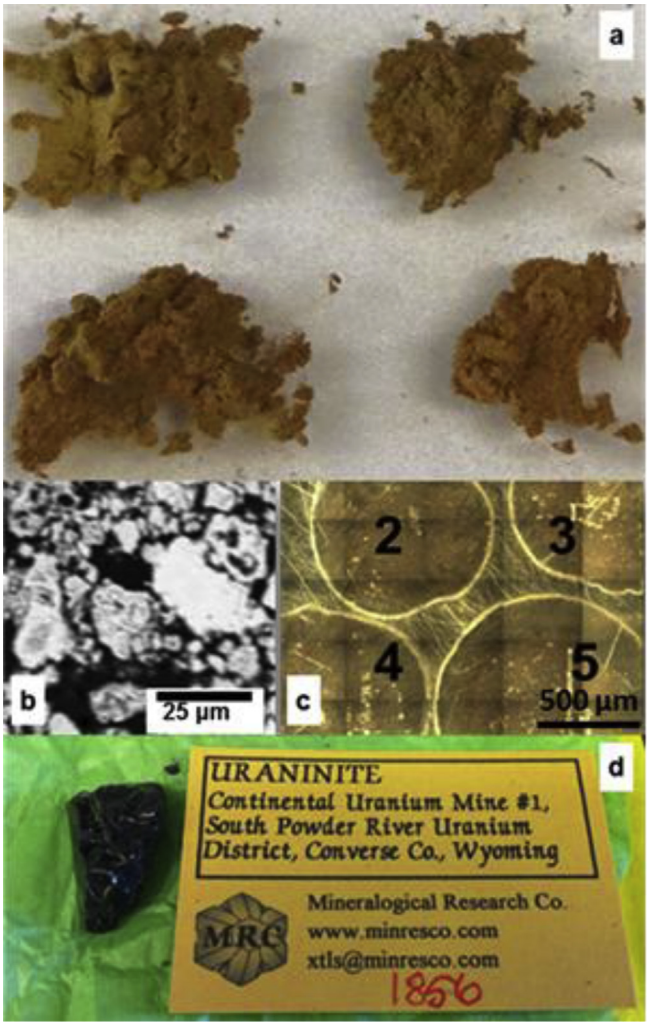

Fig. 1. **(a)** Photos depicting uranium ore concentrate powders. Clockwise from top left: sample 2, sample 3, sample 4, sample 5. **(b)** Backscatter electron image of polished epoxy-mounted uranium ore concentrate (UOC) powder. Grains are inhomogeneous with respect to size and composition as shown by variations in brightness corresponding to non-uniform distribution of U. **(c)** Epoxy-mounted UOC powder. **(d)** Uraninite from the Powder River Basin U district.

Table 1
Summary of samples analyzed in this study.

Sample Name	Type	Origin	Measurement Methods
2	Uranium Ore Concentrate	Willow Creek Project (Powder River Basin, WY)- Barrel 2, obtained from Uranium One	Electron Microprobe LA-ICP-MS SM-ICP-MS MC-ICP-MS
3	Uranium Ore Concentrate	Willow Creek Project (Powder River Basin, WY)- Barrel 3, obtained from Uranium One	Electron Microprobe LA-ICP-MS SM-ICP-MS MC-ICP-MS
4	Uranium Ore Concentrate	Willow Creek Project (Powder River Basin, WY)- Barrel 4, obtained from Uranium One	Electron Microprobe LA-ICP-MS SM-ICP-MS MC-ICP-MS
5	Uranium Ore Concentrate	Willow Creek Project (Powder River Basin, WY)- Barrel 5, obtained from Uranium One	Electron Microprobe LA-ICP-MS SM-ICP-MS MC-ICP-MS
UO_2-1	Uraninite	Continental Mine (WY), from the Mineralogical Research Corporation (www.minresco.com)	Electron Microprobe (Balboni et al., 2016) LA-ICP-MS (Balboni et al., 2016) MC-ICP-MS
UO_2-2	Uraninite	Continental Mine (WY), from the Mineralogical Research Corporation (www.minresco.com)	Electron Microprobe (Balboni et al., 2016) LA-ICP-MS (Balboni et al., 2016) MC-ICP-MS

2.2. Instrumentation

2.2.1. Trace element analysis

For SM-ICP-MS analyses, samples, standards, and blanks were analyzed in medium mass resolution mode ($M/\Delta M \approx 3000$) using an Attom (Nu Instruments) high resolution (HR)-ICP-MS instrument. Samples were also analyzed on an ELEMENT2 (Thermo Scientific) HR-ICP-MS to ensure corroborating results from elemental analyses. Results obtained with the Attom are reported and discussed here (Figs. 2–5; Table 2); a comparison of results from both instruments is contained within Supplemental Information. At the start of the analytical session, each instrument was tuned and calibrated using a multi-element solution (1 ng g^{-1}) in wet plasma mode equipped with a Meinhard concentric nebulizer and spray chamber (Scott type- ELEMENT2 and cyclonic- Attom). Additional analytical parameters employed are contained within Supplemental Information.

Laser ablation analyses were conducted on the same HR-ICP-MS instruments. Samples were ablated using a UP-213 (New Wave Research-ESI) Nd:YAG system. Background ion signals were determined for 60 s with the laser on and shuttered followed by 60 s of data acquisition. For each of the four UOC samples, 10 raster scans were completed that were ~30 μm in length with a spot size of 15 μm, 1 Hz repetition rate, and corresponding energy densities of ~8 J/cm^2. The nature of UOC samples (ultrafine powders mounted in epoxy, Fig. 1b and c), necessitated these instrumental parameters to ensure a minimum sample ablation interval (adequate counting statistics) and avoid total consumption of the powders in a short time interval.

Vanadium concentrations were determined by electron microprobe analysis of at least 10 grains within each sample and were used as an internal standard in order to monitor for instrument drift. This element was chosen as an internal standard due to its abundance (wt% level) and relatively homogeneous distribution in UOC powders. In addition to V internal standardization, every five samples were bracketed with analyses of the NIST SRM 610 glass standard reference material, which contains elements of interest at a concentration of ~500 ppm (Pearce et al., 1997). Although a matrix-matched standard such as CUP-2 UOC certified reference material (Natural Resources Canada) would be the ideal candidate for external calibration, Lach et al. demonstrated that NIST SRM glass wafers were suitable for analysis of U-rich materials (2013). The LA-ICP-MS raw data and V abundances (internal standard) are imported into the Glitter© data reduction software, which enables the selection of ion signal intervals (background and laser ablation), and consequently calculates trace element concentrations (ppm), minimum detection limits (ppm), background subtracted ion signals, and associated standard deviations (i.e., internal precision) for individual analyses (Van Achterbergh et al., 2001).

2.2.2. U isotope measurements

Uranium isotope measurements were conducted using a NuPlasma II MC-ICP-MS instrument following protocols outlined by Brennecka et al. (2010) and Bopp et al. (2010). Sample and standard solutions were self-aspirated into the plasma using a desolvating nebulizing system (DSN-100 from Nu Instruments). U isotope data were acquired in static, multi-collection mode using two Faraday collectors for measurement of ^{238}U and ^{235}U ion signals, and one discrete dynode secondary electron multiplier (SEM) for acquisition of ^{234}U. The SEM is equipped with a retardation/deceleration lens filter that limits the abundance sensitivity to ~500 ppb, whereas the latter value is < 5 ppm for all Faraday collectors as the recorded baseline measurement at mass 237 with a large ^{238}U ion signal. Analyses of CRM 112A (New Brunswick Laboratory) U isotope standard bracketed each sample so as to monitor for instrumental mass bias and drift. For standards and samples, U isotope data were collected for a total of 400 s, consisting of 40 scans of 10 s integrations each. Mass bias corrections using the exponential law were applied to samples based on the known isotopic ratios of $^{238}U/^{235}U$, $^{238}U/^{234}U$, and $^{235}U/^{234}U$ in CRM 112A. Internal in-run precision (2σ level) associated with individual U isotope measurements are typically several orders of magnitude better than the external reproducibility. The latter (relative standard deviation) reported for U isotope measurements are based on repeated analysis of CRM 112A during data acquisition for UOC and uraninite samples. Moreover, U isotope standards IRMM-184 and IRMM-185

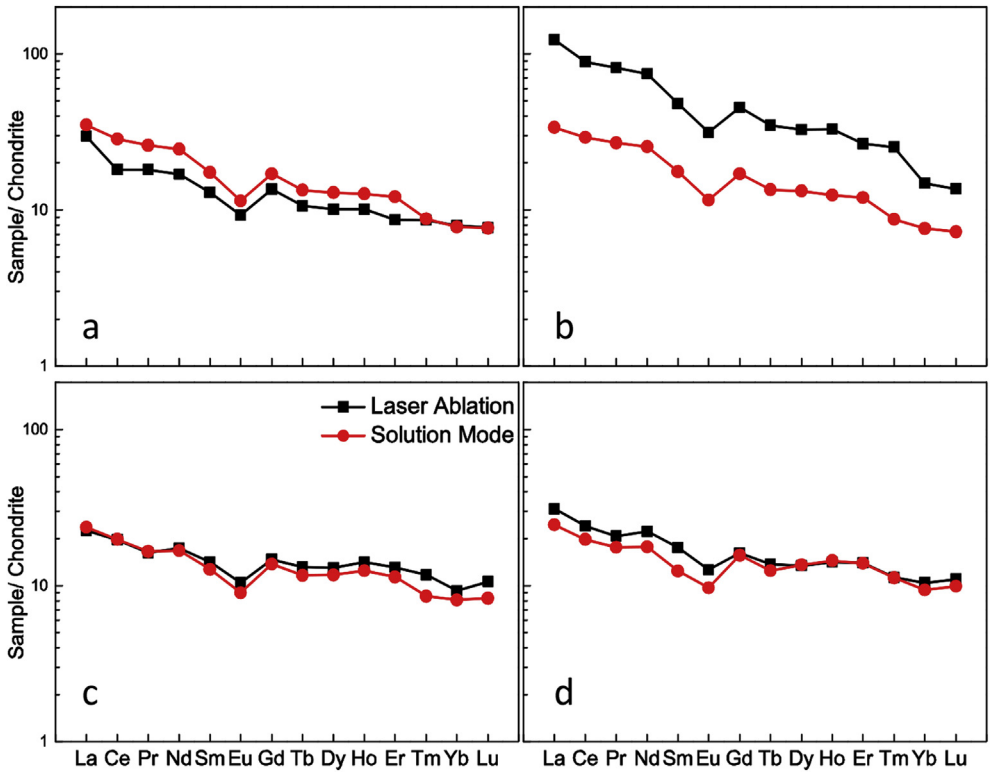

Fig. 2. Chondrite-normalized (CN) rare earth element (REE) plots for UOC sample 2 **(a)**, sample 3 **(b)**, sample 4 **(c)**, and sample 5 **(d)**. LA-ICP-MS data are shown in black and those from SM-ICP-MS data in red. Corroborating results are indicated by overlap and similar shape of CN-REE patterns for each sample regardless of introduction technique.

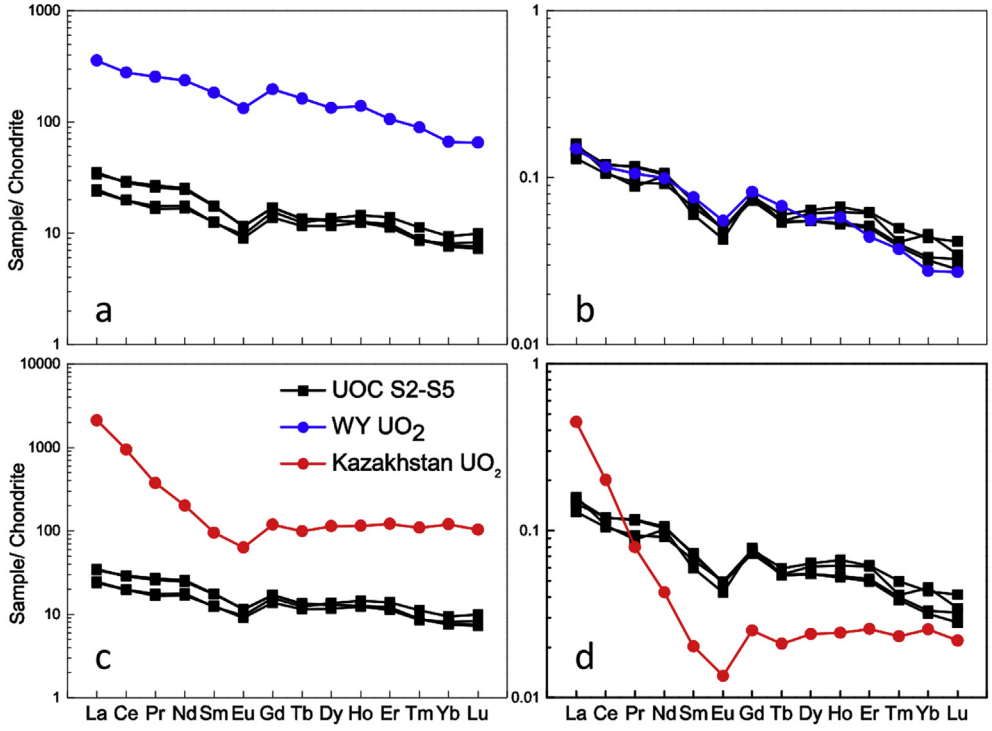

Fig. 3. **(a)** CN-REE solution mode data for UOCs samples 2–5 (black) and uraninite (blue) from the Powder River Basin U province (Balboni et al., 2016). **(b)** CN-REE data for UOC and uraninite normalized to total REE content (method after Spano et al., 2017). Patterns overlap and indicate identical origins for UOC and uraninite. **(c)** CN-REE solution mode data for UOC samples 2–5 compared with uraninite from roll-front deposits in Kazakhstan (red) (Mercadier et al., 2011). **(d)** UOC and Kazakhstan uraninite normalized to total REE content (method after Spano et al., 2017). Patterns do not overlap, despite both originating from sandstone-hosted roll front deposits. This indicates unique metalogenesis for UOC from Wyoming, and uraninite from Kazakhstan.

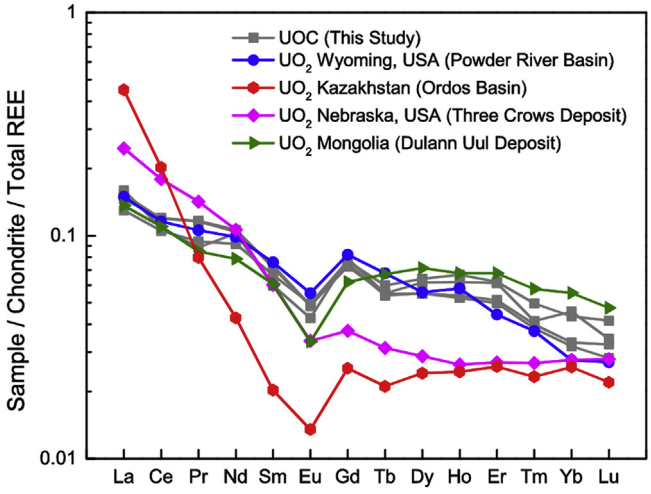

Fig. 4. REE solution mode data for UOCs samples 2–5 (grey) and uraninite (blue) from the Powder River Basin U province (Wyoming, USA) (Balboni et al., 2016), uraninite from the Chu-Sarysu Basin (Kazakhstan) (Mercadier et al., 2011), the Dulann Uul deposit in Mongolia (Lach et al., 2013), and the Three Crows deposit in Nebraska, USA (Leibold, 2013) normalized to chondrite and to total REE content (after Spano et al., 2017). All deposits are sandstone-hosted, yet variability in REE content is observed.

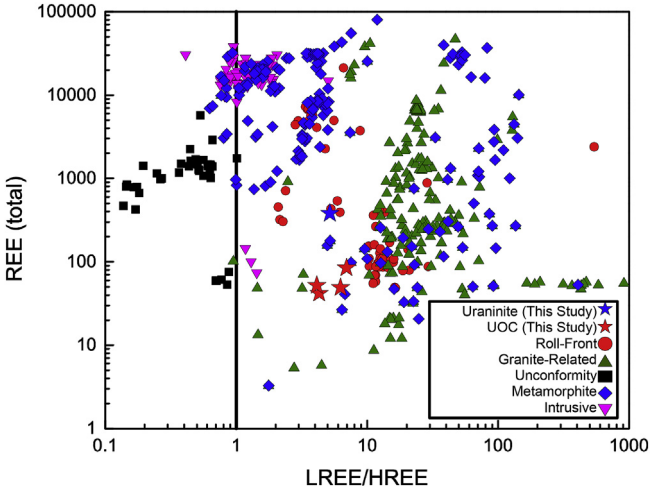

Fig. 5. Total REE content plotted as a function of LREE (La-Gd)/HREE (Tb-Lu). Values at or near 1 (vertical line) indicate no preferential incorporation of any REEs. Where LREE/HREE is less than 1, preferential incorporation of HREEs is indicated. Favoring of LREEs is shown by LREE/HREE values greater than 1. Modified from Frimmel et al. (2014). Data from Spano et al. (2017) and references within.

were also analyzed during the period of study using the same standard sample bracketing technique as that employed for the uraninite and UOC samples for method validation purposes. The results are listed in Supplemental Information and includes the calculated, average values for the U isotope ratios and their associated standard deviations (2 σ level), and these are consistent with recommended/accepted values for both standards from the literature (Condon et al., 2010; Kappel et al., 2012; Richter et al., 2005).

3. Results and discussion

3.1. Laser ablation vs. solution mode ICP-MS

Concentrations of REEs reported here (Table 2) were divided by chondritic abundances from McDonough and Sun (1995) to obtain CN values. For each of the four UOC samples, the average abundances derived from 10 ablation sites are compared with corresponding average concentrations obtained from 3 solution mode replicate analyses (Fig. 2). For solution mode analyses, the average relative uncertainty (2σ level) for each element is between ~1.5 and 8%. The LA-ICP-MS technique presents analytical challenges, which includes acquiring transient signals that result in reduced precision and accuracy relative to SM-ICP-MS analyses. Laser ablation analyses thus yielded higher average relative uncertainties (2σ level) ranging between ~10 and 30% resulting from inhomogeneous samples with respect to grain size (and thickness) and composition as shown in Fig. 1b.

Variability in REE concentrations are observed when comparing data collected using laser ablation and solution mode introduction techniques. The average concentrations obtained by LA-ICP-MS for UOC sample 2 (Fig. 2a) show slightly lower concentrations of Ce-Er when compared with REE patterns calculated using solution mode data. Conversely, UOC sample 3 displays systematically higher REE concentrations for data obtained by LA-ICP-MS (Fig. 2b). Despite these higher concentrations, of importance is that the overall shape of the pattern remains constant. Average REE patterns obtained for UOC sample 4 are virtually identical regardless of introduction technique employed (Fig. 2c). The UOC powder in sample 5 is characterized by slightly lower REE concentrations, particularly in the LREEs, than the corresponding solution mode data (Fig. 2d). Despite minor variability in CN-REE patterns resulting from different sampling strategies, the results reported in Table 2 and similar patterns shown in Fig. 2 demonstrate that LA-ICP-MS analysis is a viable alternative to the rigorous requirements involved for SM-ICP-MS methods in relation to time, material, and labor. Furthermore, corroborating results were obtained using two different HR-ICP-MS instruments (Supplemental Information), validating that valuable forensic information can be obtained regardless of sampling strategy or instrument utilized for analysis. These results expand the sampling and instrumental techniques by which U-rich materials can be characterized with no determent to the integrity of data obtained.

3.2. Forensic implications

Comparison of CN-REE signatures of UOC from this study and uraninite from the Continental Mine in the Powder River Basin investigated by Balboni et al. (2016) indicates that no fractionation of trace elements occurs during the leaching process. This is evidenced by identical CN-REE patterns obtained for uraninite and UOCs shown in Fig. 3a. Differences in absolute concentrations are observed, but when REE concentrations are normalized to total REE content (after Spano et al., 2017), the CN-REE patterns overlap (Fig. 3b) indicating that REE signatures remain viable forensic indicators subsequent to the in-situ leaching processes. In the case of U originating from the Powder River Basin, the source ore can be positively identified via corroborating REE signatures for uraninite and UOC.

REE signatures for uraninite and UOC shown in Fig. 3 indicate that the hypogene U source for the materials obtained from the Powder River Basin is likely LREE-rich monazite and other accessory minerals originating from Paleocene erosion of Precambrian granites of the Laramie Mountains (Davis, 1969). U was presumably transported in alkaline solutions enriched by tuffaceous sediments prior to deposition in the arkosic sandstones of the Wasatch formation, (Davis, 1969). Meteoric alteration of this high temperature hypogene U source would account for a lack of pronounced preferential incorporation of REEs, and results in the observed

Table 2
Trace element concentrations (ppm) for uranium ore concentrate samples.

Introduction Method	UOC Sample 2		UOC Sample 3		UOC Sample 4		UOC Sample 5	
	Solution Mode n = 3	Laser Ablation n = 10	Solution Mode n = 3	Laser Ablation n = 10	Solution Mode n = 3	Laser Ablation n = 10	Solution Mode n = 3	Laser Ablation n = 10
La	8.32	7.05	8.01	29.36	5.61	5.35	9.23	7.34
Ce	17.45	11.15	17.91	54.62	12.11	12.04	18.90	14.76
Pr	2.41	1.69	2.50	7.61	1.54	1.50	2.41	1.93
Nd	11.26	7.75	11.67	34.02	7.66	7.95	12.57	10.19
Sm	2.57	1.92	2.61	7.11	1.87	1.68	2.86	1.82
Eu	0.64	0.52	0.65	1.77	0.51	0.53	0.84	0.57
Gd	3.39	2.71	3.40	9.05	2.74	2.63	4.78	3.21
Tb	0.48	0.38	0.49	1.26	0.42	0.47	0.73	0.50
Dy	3.19	2.49	3.26	8.09	2.88	3.21	5.19	3.30
Ho	0.69	0.55	0.68	1.81	0.68	0.78	1.23	0.77
Er	1.94	1.39	1.92	4.26	1.81	2.09	3.46	2.24
Tm	0.22	0.21	0.22	0.50	0.21	0.20	0.40	0.20
Yb	1.25	1.28	1.23	2.15	1.30	1.49	2.33	1.51
Lu	0.19	0.19	0.18	0.27	0.20	0.21	0.38	0.19

relatively flat but slightly light rare earth element (LREE) enriched CN-REE patterns (Frimmel et al., 2014; Mercadier et al., 2011). A negative Eu anomaly is observed for samples analyzed here, and can be attributed to the presence of Eu^{2+} in a reducing magma. Consequently, this enables Eu^{2+} to substitute for Ca^{2+} and is thus indicative of early crystal fractionation of plagioclase in silicate melts (Frimmel et al., 2014; Weill and Drake, 1973); this further suggests a granitic primary source of U that mobilized and reduced to form the roll-front deposits of the Powder River Basin.

Distinguishing between U ore sources is an essential goal of nuclear forensics. To this end, the REE signatures observed for UOCs in this study are compared to those for roll-front-hosted U from Kazakhstan (Fig. 3c) as reported by Mercadier et al. (2011). The latter signatures are characterized by LREE (La-Gd) enrichment and a negative Eu anomaly. Powder River Basin (PRB) UOCs display less LREE enrichment and higher relative heavy REE (HREE) content than Kazakhstan U (Fig. 3d), which may be attributable to differences in the salinity, temperature, and supergene REE source during formation (Mercadier et al., 2011). These differences in ore formation mechanisms for deposits of the same genetic type originating from two localities (Kazakhstan and the United States) are corroborated by distinct CN-REE patterns shown in Fig. 3c. Differences in provenance are further evidenced by dissimilar patterns when REE signatures for Kazakhstan uraninite and UOC from this study are normalized to total REE content (Fig. 3d). No overlap of signatures is observed, which is contrary to the case for REE signatures for uraninite and UOC derived from the same locality (Fig. 3b).

CN-REE content of uraninite for roll-front uraninite from the Three Crows region of Nebraska (United States) (Leibold, 2013), and the Dulann Uul deposit in Mongolia (Lach et al., 2013) were also compared to those for UOC and uraninite examined in this study (Fig. 4). Once again, CN values for each REE were normalized to total REE content to qualitatively examine the degree of similarity to U-rich materials in this study (Spano et al., 2017). Uraninite from the Three Crows deposit displays a REE pattern distinct from that of uraninite and UOC from this study. A greater degree of LREE enrichment and HREE depletion for this deposit indicates an origin that differs from that of the Powder River Basin (Leibold, 2013). Some overlap of the signature from the Dulan Uul deposit is observed, but is distinguished from uraninite and UOC from the Powder River Basin by a more prominent negative Eu anomaly. A lesser degree of HREE depletion is also observed for this uraninite. The similarities in the REE signature from Dulaan Uul to those of UOC and uraninite from the Powder River Basin are expected as both deposits have similar geochemical origins (Lach et al., 2013).

Preferential incorporation of LREEs or HREEs were interpreted as a means of differentiating between different deposit types (Frimmel et al., 2014; Mercadier et al., 2011). In Fig. 5, the sum of REE concentrations are plotted as a function of the total of all LREEs (La-Gd) divided by the total of all HREEs (Tb-Lu). When LREE/HREE values are close to one, deposits with high-temperature origins (such as intrusive, and some metamorphic deposits) are indicated resulting from ionic-radius independent incorporation of REEs. Uraninite may incorporate all REEs regardless of size at higher temperatures, whereas at lower temperatures it preferentially incorporates elements having a similar ionic radius to U^{4+} in eight-fold coordination (Mercadier et al., 2011).

For samples with LREE/HREE <1, lower temperature deposits are indicated as uraninite more easily incorporates mid-to-heavy REEs as is commonly the case in unconformity deposits (Spano et al., 2017). This trend towards preferential incorporation of mid to heavy REEs in unconformity type deposits is further illustrated in Fig. 5. LREE/HREE distributions in metamorphite deposits appear to have a bimodal distribution, possibly related to high (LREE/HREE ~1) and low (LREE/HREE >> 1) temperature diagenesis. Furthermore, REE partitioning within metamorphite-related U deposits spans nearly four orders of magnitude, indicating complex and diverse metallogenesis.

Light-to-mid REE enrichment results in LREE/HREE values greater than one, and is observed in UOC and uraninite samples from this study, along with those from roll-front, metamorphite, and granite-related U deposits (Fig. 5; modified after Frimmel et al., 2014; data from Spano et al., 2017 and references within). The granitic hypogene origin of U that altered to form roll-front type uraninite and corresponding UOCs investigated in this study is evidenced by an intermediate LREE/HREE, signature which is in the range of other roll front deposits, and proximal to granite-related and metamorphite deposits (Fig. 5; Dahlkamp, 1993).

3.3. Uranium isotope measurements: results and forensic implications

Four samples of UOC and two specimens of uraninite from the Powder River Basin U province yield average $^{238}U/^{235}U$ ratios and associated external reproducibility (2σ level) of 137.788 ± 0.049 and 137.888 ± 0.049, respectively. Average (and associated 2σ external reproducibility) $^{235}U/^{234}U$ ratios are 131.3 ± 2.4 and 134.8 ± 2.4 for UOC and uraninite, respectively, whereas $^{238}U/^{234}U$ ratios are 18,106 ± 641 for UOC and 18,415 ± 641 for uraninite.

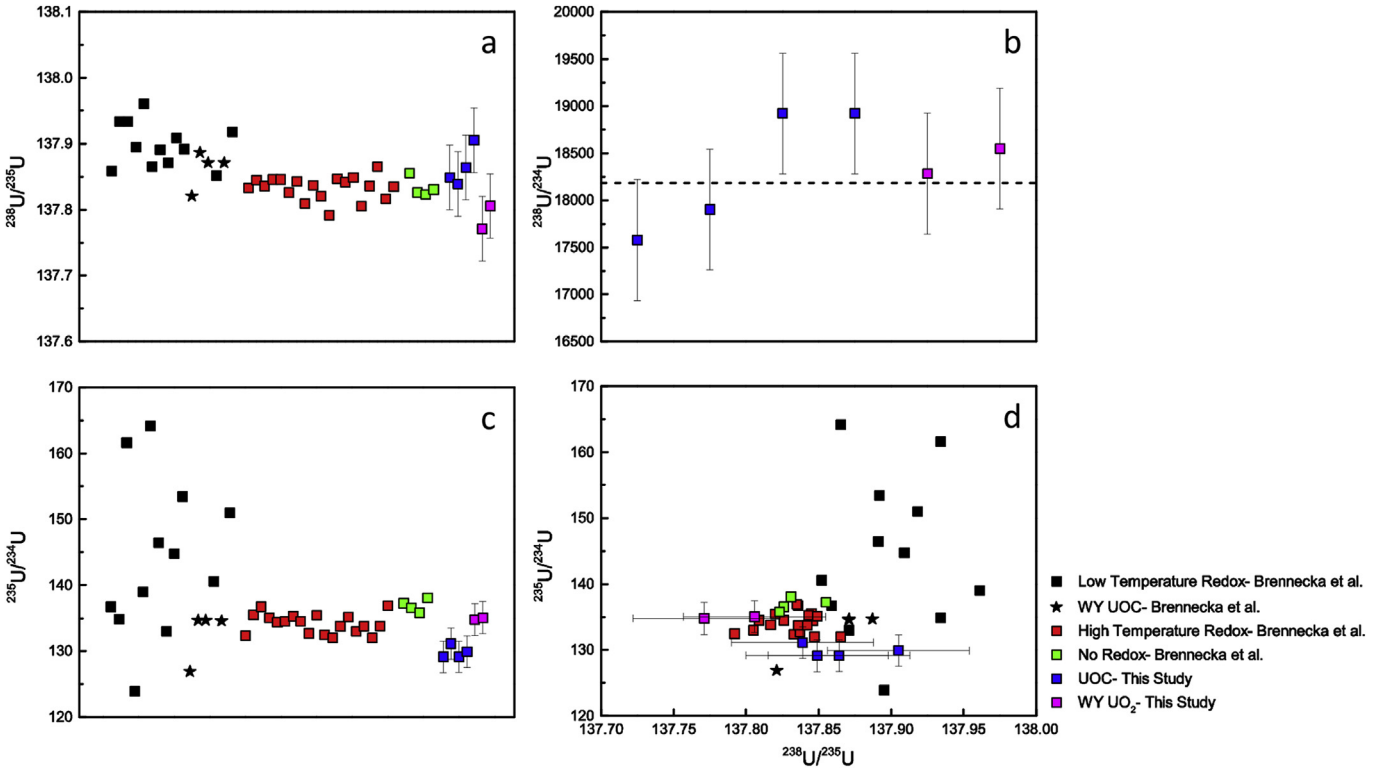

Fig. 6. **(a–c)** U isotope data for uranium ore concentrate (UOC) and uraninite from this study compared to UOC from low, high, and no-redox related U deposits worldwide. Secular equilibrium for $^{238}U/^{234}U$ is indicated by dashed line (Keegan et al., 2008). **(d)** $^{235}U/^{234}U$ plotted as a function of $^{238}U/^{235}U$. Star data points correspond to the U isotope composition for UOC from the Powder River Basin U province as determined by Brennecka et al. (2010).

Data obtained in this study are compared with values reported by Brennecka et al. (2010) for $^{238}U/^{235}U$ and $^{235}U/^{234}U$ isotope systems in UOCs. In Fig. 6a, c, and d, data are shown for UOC from low temperature redox-related deposits, and include those from roll front and black shale type U deposits. Also shown for comparison are UOC originating from high temperature redox sensitive ores including those from unconformity, vein-type, intrusive, metamorphic and collapse-breccia pipe type deposits (Fig. 6a, c, and d). UOC from quartz-pebble conglomerate-hosted U deposits are also displayed and these represent non-redox sensitive U sources (Brennecka et al., 2010).

The measured $^{238}U/^{235}U$ signatures for both UOC and WY uraninite from this study overlap (given their associated external reproducibility at 2σ level; Fig. 6a), indicating that forensic signatures for this isotope pair persist beyond in-situ leaching. These signatures are also similar to other samples of UOC from WY U deposits (Fig. 6a; Brennecka et al., 2010). Additionally, $^{238}U/^{234}U$ ratios also overlap given their respective external reproducibility (2σ), and thus no observable fractionation occurred in the transformation from uraninite to UOC (Fig. 6b). Average $^{235}U/^{234}U$ ratios for uraninite and corresponding UOCs also overlap given their external reproducibility at the 2σ level (Fig. 6c). As observed in the $^{238}U/^{235}U$ system, $^{235}U/^{234}U$ signatures of uraninite and UOC from this study are similar to those of WY UOCs reported by Brennecka et al. (2010 Fig. 6c).

Plotting $^{235}U/^{234}U$ vs. $^{238}U/^{235}U$ corroborates the validity of using U isotope ratios to constrain depositional redox and water/rock interactions as forensic signatures. This method also exploits differences in fractionation mechanisms (NFS vs. mass dependent) for these isotope systems as evidenced by a lack of correlation between $^{235}U/^{234}U$ and $^{238}U/^{235}U$ ratios (Brennecka et al., 2010). Fig. 6d shows that the UOCs and uraninite investigated here exhibit a greater variability in $^{238}U/^{235}U$ ratios, while $^{235}U/^{234}U$ values are relatively well constrained. The U isotope compositions of UOC and uraninite analyzed in this study are similar to those for uraninite of low temperature origin, and are especially consistent with previously reported values for UOC originating in WY (Fig. 6d). These results indicate that all three isotope systems can provide information about deposition and alteration conditions associated with uraninite, and that $^{238}U/^{235}U$, $^{238}U/^{234}U$, and $^{235}U/^{234}U$ do not undergo isotopic fractionation during early ore processing.

4. Conclusions

The time required for analyzing forensic signatures in U-rich materials can be significantly reduced by employing a LA-ICP-MS technique, while still obtaining validated and accurate trace element concentrations. Near-identical REE signatures are observed in analyzed UOC samples when compared to the primary uraninite from which the UOC originated signifying a lack of REE partitioning during processing. In this study, UOC is attributable to a specific locality containing roll-front hosted U when considering REE and U isotope signatures. Furthermore, $^{238}U/^{235}U$, $^{238}U/^{234}U$, and $^{235}U/^{234}U$ values reported here indicate that these systems remain viable indicators of redox effects and water rock interactions on U ore genesis and these signatures persist in the conversion to UOC from uraninite.

Acknowledgements

Funding for this project was provided by the Department of Homeland Security Domestic Nuclear Detection Office Academic Research Initiative (DHS-14-DN-077-ARI-01). The authors also wish to acknowledge Dr. Ian Steele for his assistance in operating the

electron microprobe, and Nina Jones and Bianca Monaco for their assistance with U ion exchange column chemistry.

Appendix A. Supplementary data

Supplementary data related to this article can be found at http://dx.doi.org/10.1016/j.apgeochem.2017.07.003.

References

Abe, M., Suzuki, T., Fujii, Y., Hada, M., Hirao, K., 2008. An ab initio molecular orbital study of the nuclear volume effects in uranium isotope fractionations. J. Chem. Phys. 129, 164309.

Balboni, E., Jones, N., Spano, T., Simonetti, A., Burns, P.C., 2016. Chemical and Sr isotopic characterization of North America uranium ores: nuclear forensic applications. Appl. Geochem. 74, 24–32.

Bigeleisen, J., 1996. Nuclear size and shape effects in chemical reactions. Isotope chemistry of the heavy elements. J. Am. Chem. Soc. 118, 3676–3680.

Bopp, C.J., Lundstrom, C.C., Johnson, T.M., Sanford, R.A., Long, P.E., Williams, K.H., 2010. Uranium 238U/235U isotope ratios as indicators of reduction: results from an in situ biostimulation experiment at Rifle, Colorado, U.S.A. Environ. Sci. Technol. 44, 5927.

Boulyga, S., Konegger-Kappel, S., Richter, S., Sangely, L., 2015. Mass spectrometric analysis for nuclear safeguards. J. Anal. Atomic Spectrom. 30, 1469–1489.

Boulyga, S.F., Koepf, A., Konegger-Kappel, S., Macsik, Z., Stadelmann, G., 2016. Uranium isotope analysis by MC-ICP-MS in sub-ng sized samples. J. Anal. Atomic Spectrom. 31, 2272–2284.

Bowie, S.H.U., 1979. The Mode of Occurrence and Distribution of Uranium Deposits.

Brennecka, G.A., Borg, L.E., Hutcheon, I.D., Sharp, M.A., Anbar, A.D., 2010. Natural variations in uranium isotope ratios of uranium ore concentrates: understanding the 238U/235U fractionation mechanism. Earth Planet. Sci. Lett. 291, 228–233.

Condon, D.J., McLean, N., Noble, S.R., Bowring, S.A., 2010. Isotopic composition (238 U/235 U) of some commonly used uranium reference materials. Geochimica Cosmochimica Acta 74, 7127–7143.

Dahl, A.R., Hagmaier, J.L., 1976. Genesis and Characteristics of the Southern Powder River Basin Uranium Deposits. Guidebook - Wyoming Geological Association, Wyoming, pp. 243–252.

Dahlkamp, F.J., 1993. Uranium Ore Deposits. Springer-Verlag.

Davis, J.F., 1969. Uranium deposits of the Powder River basin. Rocky Mt. Geol. 8, 131–141.

Depiné, M., Frimmel, H.E., Emsbo, P., Koenig, A.E., Kern, M., 2013. Trace element distribution in uraninite from Mesoarchaean Witwatersrand conglomerates (South Africa) supports placer model and magmatogenic source. Min. Deposita 48, 423–435.

Dhana Raju, R., Babu, E.V.S.S.K., 2003. REE geochemistry of the uranium phases in syn- magmatic and hydrothermal-type U-mineralisation; two case histories from India. J. Geol. Soc. India 62, 23–35.

Dustin, M.K., Koeman, E.C., Simonetti, A., Torrano, Z., Burns, P.C., 2016. Comparative investigation between in situ laser ablation versus bulk sample (solution mode) inductively coupled plasma mass spectrometry (ICP-MS) analysis of trinitite post-detonation materials. Appl. Spectrosc. 70 (9).

Finch, R., Murakami, T., 1999. Systematics and paragenesis of uranium minerals. Rev. Mineralogy Geochem. 38, 91–179.

Finch, W.I., 1996. Uranium Provinces of North America- Their Definition, Distribution, and Models. U.S. Geological Survey Bulletin, Washington, D.C.

Fleischer, M., Altschuler, Z.S., 1969. The relationship of the rare- earth composition of minerals to geological environment. Geochimica Cosmochimica Acta 33, 725–732.

Frimmel, H.E., Schedel, S., Brätz, H., 2014. Uraninite chemistry as forensic tool for provenance analysis. Appl. Geochem. 48, 104–121.

Fryer, B.J., Taylor, R.P., 1987. Rare- earth element distributions in uraninites: implications for ore genesis. Chem. Geol. 63, 101–108.

Han, S.-H., Varga, Z., Krajko, J., Wallenius, M., Song, K., Mayer, K., 2013. Measurement of the sulphur isotope ratio (34S/32S) in uranium ore concentrates (yellow cakes) for origin assessment. J. Anal. Atomic Spectrom. 28, 1919–1925.

Horie, K., Tsutsumi, Y., Cho, M., Morishita, Y., Hidaka, H., 2010. Crystallization of REE minerals and redistribution of U, Th, and REE at contact boundary between granite and gabbro during hydrothermal alteration. Phys. Chem. Earth 35, 284–291.

IAEA, 2006. Nuclear forensics support. In: Series, I.N.S. (Ed.), IAEA Nuclear Security Series. International Atomic Energy Association Vienna, Austria.

IAEA, 2014. Uranium 2014: Resources, Production and Demand.

Jenner, G.A., Longerich, H.P., Jackson, S.E., Fryer, B.J., 1990. ICP-MS — a powerful tool for high-precision trace-element analysis in Earth sciences: evidence from analysis of selected U.S.G.S. reference samples. Chem. Geol. 83, 133–148.

Kappel, S., Boulyga, S.F., Prohaska, T., 2012. Direct uranium isotope ratio analysis of single micrometer-sized glass particles. J. Environ. Radioact. 113, 8–15.

Keegan, E., Kristo, M.J., Colella, M., Robel, M., Williams, R., Lindvall, R., Eppich, G., Roberts, S., Borg, L., Gaffney, A., Plaue, J., Wong, H., Davis, J., Loi, E., Reinhard, M., Hutcheon, I., 2014. Nuclear forensic analysis of an unknown uranium ore concentrate sample seized in a criminal investigation in Australia. Forensic Sci. Int. 240, 111–121.

Keegan, E., Richter, S., Kelly, I., Wong, H., Gadd, P., Kuehn, H., Alonso-Munoz, A., 2008. The provenance of Australian uranium ore concentrates by elemental and isotopic analysis. Appl. Geochem. 23, 765–777.

Keegan, E., Wallenius, M., Mayer, K., Varga, Z., Rasmussen, G., 2012. Attribution of uranium ore concentrates using elemental and anionic data. Appl. Geochem. 27, 1600–1609.

Krajkó, J., Varga, Z., Wallenius, M., Mayer, K., 2016. Pre-concentration of trace levels of rare-earth elements in high purity uranium samples for nuclear forensic purposes. Radiochim. Acta 471.

Lach, P., Mercadier, J., Dubessy, J., Boiron, M.C., Cuney, M., 2013. In situ quantitative measurement of rare earth elements in uranium oxides by laser ablation-inductively coupled plasma-mass spectrometry. Geostand. Geoanal. Res. 37, 277–296.

Leibold, J., 2013. Geochemistry and Mineralogy of the Alteration Halo Associated with the Three Crow Roll-front Uranium Deposit. Colorado School of Mines, Nebraska, USA.

Martin, B., 1980. In Situ Leaching of Uranium.

Mayer, K., Wallenius, M., Fanghänel, T., 2007. Nuclear forensic science—from cradle to maturity. J. Alloys Compd. 444, 50–56.

Mayer, K., Wallenius, M., Ray, I., 2005. Nuclear forensics—a methodology providing clues on the origin of illicitly trafficked nuclear materials. Analyst 130, 433–441.

McDonough, W.F., Sun, S.s, 1995. The composition of the Earth. Chem. Geol. 120, 223–253.

Mercadier, J., Cuney, M., Lach, P., Boiron, M.C., Bonhoure, J., Richard, A., Leisen, M., Kister, P., 2011. Origin of uranium deposits revealed by their rare earth element signature. Terr. Nova 23, 264–269.

Nations, U., 1968. Treaty on the Non-proliferation of Nuclear Weapons (NPT). United Nations Treaty Series.

Pearce, N.J., Perkins, W.T., Westgate, J.A., Gorton, M.P., Jackson, S.E., Neal, C.R., Chenery, S.P., 1997. A compilation of new and published major and trace element data for NIST SRM 610 and NIST SRM 612 glass reference materials. Geostand. Newsl. 21, 115–144.

Pollington, A.D., Kinman, W.S., Hanson, S.K., Steiner, R.E., 2016. Polyatomic interferences on high precision uranium isotope ratio measurements by MC-ICP-MS: applications to environmental sampling for nuclear safeguards. J. Radioanalytical Nucl. Chem. 307, 2109–2115.

Premadas, A., Srivastava, P.K., 2002. Inductively coupled plasma atomic emission spectrometric determination of lanthanides and Y in various uranium hydrometallurgical products. J. Radioanalytical Nucl. Chem. 251, 233–239.

René, M., 2008. Anomalous rare earth element, yttrium and zirconium mobility associated with uranium mineralization. Terra Nova. 20, 52–58.

Richter, S., Alonso, A., De Bolle, W., Kühn, H., Verbruggen, A., Wellum, R., Taylor, P., 2005. Re-certification of a series of uranium isotope reference materials: IRMM-183, IRMM-184, IRMM-185, IRMM-186 and IRMM-187. Int. J. Mass Spectrom. 247, 37–39.

Richter, S., Alonso, A., De Bolle, W., Wellum, R., Taylor, P.D.P., 1999. Isotopic "fingerprints" for natural uranium ore samples. Int. J. Mass Spectrom. 193, 9–14.

Santos, E.S., Ludwig, K.R., 1983. Age of uranium mineralization at the Highland Mine, Powder River basin, Wyoming, as indicated by U-Pb isotope analyses. Econ. Geol. Bull. Soc. Econ. Geol. 78, 498–501.

Society, J.W.G.o.t.A.P., 2008. In: Society, J.W.G.o.t.A.P. (Ed.), Nuclear Forensics Role, State of the Art, Program Needs. American Physical Society, USA.

Spano, T.L., Simonetti, A., Wheeler, T., Carpenter, G., Freet, D., Balboni, E., Dorais, C., Burns, P.C., 2017. A novel nuclear forensic tool involving deposit type normalized rare earth element signatures. Terra Nova 1–12. https://doi.org/10.1111/ter.12275.

Stirling, C.H., Andersen, M.B., Potter, E.-K., Halliday, A.N., 2007. Low-temperature isotopic fractionation of uranium. Earth Planet. Sci. Lett. 264, 208–225.

Švedkauskaite-legore, J., Mayer, K., Millet, S., Nicholl, A., Rasmussen, G., Baltrunas, D., 2007. Investigation of the isotopic composition of lead and of trace elements concentrations in natural uranium materials as a signature in nuclear forensics. Ract 95, 601–605.

Van Achterbergh, E., Ryan, C., Jackson, S., Griffin, W., 2001. Data reduction software for LA-ICP-MS. In: Sylvester, P. (Ed.), Laser Ablation—ICP-mass Spectrometry in the Earth Sciences: Principles and Applications.

Varga, Z., Wallenius, M., Mayer, K., 2010. Origin assessment of uranium ore concentrates based on their rare-earth elemental impurity pattern. Radiochimica Acta Int. J. Chem. Aspects Nucl. Sci. Technol. 98, 771–778.

Walters, A.S., Goodenough, K.M., Hughes, H.S.R., Roberts, N.M.W., Gunn, A.G., Rushton, J., Lacinska, A., 2013. Enrichment of rare earth elements during magmatic and post-magmatic processes: a case study from the loch loyal syenite complex, northern Scotland. Contrib. Mineral. Pet. 166, 1177–1202.

Weill, D.F., Drake, M.J., 1973. Europium anomaly in plagioclase feldspar: experimental results and semiquantitative model. Science 180, 1059–1060.